THE JOURNAL OF PHYSICAL CHEMISTRY LETTERS
A JOURNAL OF THE AMERICAN CHEMICAL SOCIETY

pubs.acs.org/JPCL Letter

Electron Affinities of Ligated Icosahedral M_{13} Superatoms Revisited by Gas-Phase Anion Photoelectron Spectroscopy

Shun Ito, Yuriko Tasaka, Katsunosuke Nakamura, Yuki Fujiwara, Keisuke Hirata, Kiichirou Koyasu, and Tatsuya Tsukuda*

Cite This: *J. Phys. Chem. Lett.* 2022, 13, 5049−5055 Read Online

ACCESS | Metrics & More | Article Recommendations | Supporting Information

ABSTRACT: The electron binding energies of the ligand-protected gold/silver-based cluster anions, $[Au_{25}(SR)_{18}]^-$, $[XAg_{24}(SR')_{18}]^{2-}$ (X = Ag^+, Au^+, Pd^0, or Pt^0), and $[PdAu_{24}(C{\equiv}CR'')_{18}]^{2-}$ having icosahedral M_{13} superatomic cores, were reexamined by gas-phase photoelectron spectroscopy (PES) on a significantly intensified mass-selected ion beam. Laser fluence-dependent PE spectra and pump−probe PES revealed that the previous PE spectra were contaminated by PE signals due to the two-photon electron detachment via long-lived photoexcited states. Although the adiabatic electron affinities (AEAs) of the corresponding oxidized forms were found to be 1−2 eV larger than those previously reported, the effects of doping and ligation were not qualitatively affected. (1) The AEA of the Ag_{13} superatom (∼4 eV) was not appreciably affected by doping a Au atom at the center but was reduced by ∼2 eV by doping Pd or Pt, and (2) the AEA of $PdAu_{12}$ protected by $Au_2(C{\equiv}CR'')_3$ units was much larger than that of $PdAg_{12}$ protected by $Ag_2(SR')_3$ units.

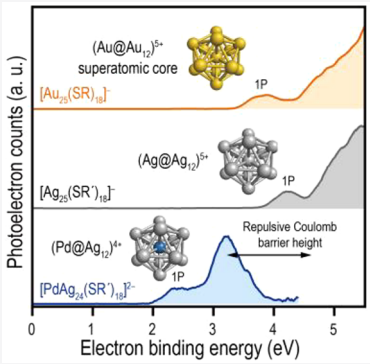

Ligand-protected gold/silver clusters with precisely defined compositions and structures constitute a growing class of nanomaterials with unique physicochemical properties.[1−10] Their intrinsic stabilities and novel properties are intimately related to the electronic structures, which are sensitive to geometric structures and rationalized by the superatomic concept.[1,11,12] In this model, the valence electrons are accommodated in quantized superatomic orbitals (1S, 1P, 1D, 2S, etc.) distributed over the metallic cores and the protected clusters gain a special stability when the electronic shells are closed. Thus, it is important to understand how the electronic structures can be manipulated by changing structural parameters such as the size, the geometric structures and composition of the cores, the total charge of the clusters, and the nature of the ligands for the rational development of functional clusters.

A promising approach for establishing the design principles of electronic structures is gas-phase photoelectron spectroscopy (PES)[13−20] on ligand-protected Au/Ag cluster anions whose geometric structures were determined by X-ray crystallography. Since 2017,[13] we have applied PES to representative ligand-protected Au/Ag superatoms, including $[Au_{25}(PET)_{18}]^-$ (**1**$^-$; PET = 2-$C_6H_5C_2H_4S$),[21,22] $[XAg_{24}(DMBT)_{18}]^{2-}$ [**2**$^-$, **3**$^-$, **4**$^{2-}$, and **5**$^{2-}$ for X = Ag^+, Au^+, Pd^0, and Pt^0, respectively; DMBT = 2,4-$(CH_3)_2C_6H_3S$],[23−25] and $[PdAu_{24}(C{\equiv}CAr^F)_{18}]^{2-}$ [**6**$^{2-}$; $C{\equiv}CAr^F$ = 3,5-$(CF_3)_2C_6H_3C{\equiv}C$].[26] The crystal structures of **1**$^-$−**6**$^{2-}$ are anatomically divided into the superatomic cores and surrounding ligand shells, as shown in Table 1. Clusters **1**$^-$−**6**$^{2-}$ have icosahedral M_{13} superatomic cores with a closed electron shell configuration $(1S)^2(1P)^6$. Using PES for these 8e superatoms, we studied how the adiabatic electron affinities (AEAs) of the corresponding 7e superatoms are affected by the composition of the cores, the total charge of the clusters, and the nature of the ligands (Table 1). The AEAs of **1**^{0}, **2**^{0}, and **3**^{0} were previously determined to be 2.36, 2.02, and 2.08 eV, respectively, indicating that the electronic structure of icosahedral M_{13} does not depend so much on whether M is Au or Ag.[14,15] In contrast, the AEAs of Pd/Pt-doped anions **4**$^-$ and **5**$^-$ (0.61 and 0.60 eV, respectively) were significantly smaller than that of undoped **2**^{0} (2.02 eV).[15] This doping effect was explained by the reduction of the formal charge in the core potential upon the replacement of Ag^+ with X^0 (X = Pd and Pt) and/or the upward shift of the apparent vacuum level by the presence of a repulsive Coulomb barrier (RCB)[27,28] between the detached electron and remaining anions **4**$^-$ and **5**$^-$. The AEA of **6**$^-$ was 2.15 eV and was reduced by ∼80 meV by the stepwise replacement of a $C{\equiv}CAr^F$ ligand with C≡CPh. This result demonstrates that the CF_3 groups on the $C{\equiv}CAr^F$ ligand played a crucial role in the electronic stabilization of **6**$^{2-}$.[20] Table 1 also lists the calculated AEA values of **1**^{0}, **2**^{0}, **3**^{0}, **4**$^-$, and **5**$^-$. All of the reported experimental

Received: April 29, 2022
Accepted: May 27, 2022
Published: June 2, 2022

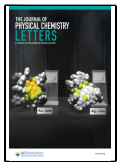

https://doi.org/10.1021/acs.jpclett.2c01284
J. Phys. Chem. Lett. 2022, 13, 5049−5055

Table 1. Ligand-Protected Gold/Silver Clusters Used in This Study

Cluster	$[Au_{25}(PET)_{18}]^-$ (**1**$^-$)	$[XAg_{24}(DMBT)_{18}]^{2-}$ X = Ag^+ (**2**$^-$)	Au^+ (**3**$^-$)	Pd^0 (**4**$^{2-}$)	Pt^0 (**5**$^{2-}$)	$[PdAu_{24}(C{\equiv}CAr^F)_{18}]^{2-}$ (**6**$^{2-}$)
Ligand shell	6 × $Au_2(PET)_3$	6 × $Ag_2(DMBT)_3$				6 × $Au_2(C{\equiv}CAr^F)_3$
Superatomic core	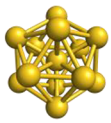	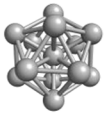	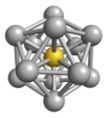	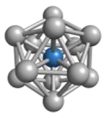	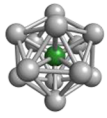	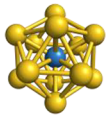
	$Au@Au_{12}$[a]	$X@Ag_{12}$[b]				$Pd@Au_{12}$[c]
AEA_{exp} (eV)[d]	2.36[e]	2.02[f]	2.08[f]	0.61[f]	0.60[f]	2.15[g]
AEA_{cal} (eV)[h]	2.94[i] / 3.23[j]	3.46[f,k]	3.51[f,k]	1.17[f,k]	1.22[f,k]	N.A.
AEA_{exp} (eV)[l]	3.45	3.97	4.00	2.00	2.08	3.20

[a]From refs 21 and 22. [b]From refs 23−25. [c]From ref 26. [d]Experimental AEAs of the ionized forms determined previously. [e]From ref 14. [f]From ref 15. [g]From ref 20. [h]Theoretical AEAs of the oxidized forms reported previously. [i]From ref 29. [j]From ref 30. [k]Ligands were simplified as SCH_3. [l]Experimental AEAs of the corresponding oxidized forms determined in the study presented here.

AEA values were significantly (∼0.6−1.4 eV) smaller than the calculated AEAs.[15,29,30]

In our previous studies,[13−15,18,20] a high-fluence laser was used to measure the PE spectra of **1**$^-$−**6**$^{2-}$ because of the small beam intensities of the target cluster anions: the duty cycle of pulsed extraction from the continuous electrospray ionization (ESI) beam to the time-of-flight mass spectrometer (TOF-MS) was only ∼0.2%. Such a setup forced us to spend several hours recording the PE spectra and prevented us from studying the laser fluence dependence of the PE signals to avoid multiphoton processes. To remedy this situation, we recently installed an ion trap as an interface between the continuous ESI source and pulsed TOF-MS[31] to increase the ion intensities by ∼2 orders of magnitude. The purpose of this study was to remeasure the PE spectra of **1**$^-$−**6**$^{2-}$ using the updated apparatus. We found that the previously reported AEAs were underestimated due to the involvement of PE detachment from photoexcited states. The AEAs were redetermined from the PE spectra recorded at a smaller laser fluence to suppress the multiphoton processes (Table 1).

The black trace in Figure 1a represents the PE spectrum of **1**$^-$ measured at 266 nm (4.66 eV) at a fluence of 25 mJ cm^{-2}; the fluence was comparable to that used in the previous report.[14] The spectrum shows a main band in the region of electron binding energy (E_{eb}) of >3.5 eV (termed band II) and a small band in the lower E_{eb} region with a tailed structure (termed band I). The onset energies of bands I and II (E_I and E_{II}, respectively) were 2.32 ± 0.06 and 3.45 ± 0.06 eV, respectively. While the E_I value reproduced that reported previously (2.36 eV), the profile of band II differed from that reported previously[14] due to the remarkable improvement in the S/N ratio in the E_{eb} region of >4 eV. The PE spectral profile recorded at 266 nm was significantly dependent on the laser fluence; the relative intensity of band I with respect to band II decreased at a fluence of 0.5 mJ cm^{-2} (red trace in Figure 1a). This laser fluence dependence suggests that multiple photons were involved in band I. To test this hypothesis, the PE counts for bands I and II were plotted against the laser fluences in a double-logarithmic plot (Figure 2). The slope of the plot corresponds to the number of photons involved in PE detachment under the condition that the fraction of the parent ions depleted by photoirradiation is negligibly small (Supporting Information). While one-photon electron detachment was confirmed in the reference experiment with I^- (Figure S2a,b), the slope for band I (1.17 ± 0.02) at 266 nm was <2 but obviously larger than that for band II

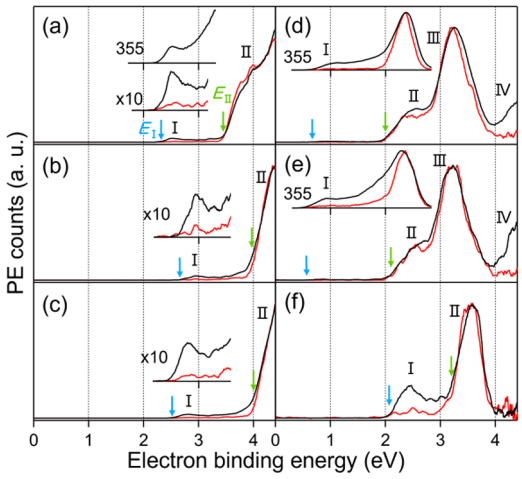

Figure 1. PE spectra of (a) **1**$^-$, (b) **2**$^-$, (c) **3**$^-$, (d) **4**$^{2-}$, (e) **5**$^{2-}$, and (f) **6**$^{2-}$ measured at 266 nm. The insets of panels a−c show enlarged views of band I. PE spectra recorded at 355 nm are shown in the insets of panels a, d, and e. The black traces were recorded at a laser fluence of 25 mJ cm^{-2}, whereas the red traces were recorded at fluences of 0.5 and 1.0 mJ cm^{-2} for panels a−e and panel f, respectively. Blue and green arrows show E_I and E_{II}, respectively.

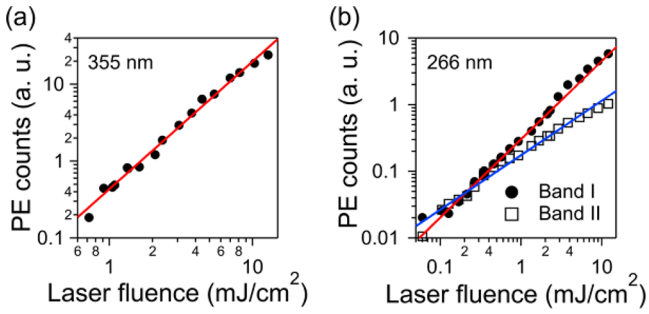

Figure 2. Double-logarithmic plots and fitting lines for the PE counts of **1**$^-$ plotted against the laser fluences at (a) 355 nm and (b) 266 nm.

(0.82 ± 0.03) (Figure 2b). The slope for band I at 355 nm was 1.66 ± 0.04 (Figure 2a). These results led us to conclude that band I originated from a two-photon process whereas band II was due to a direct PE detachment (Scheme 1a). To help with the assignment, the PE spectrum of **1**$^-$ was measured at 193 nm (red-shaded area in Figure 3a); band II was assigned to the PE signals from the HOMO (1P superatomic orbital), and band III was assigned to the Au(5d) band. Band II at 266 nm

https://doi.org/10.1021/acs.jpclett.2c01284
J. Phys. Chem. Lett. 2022, 13, 5049−5055

Scheme 1. PE Detachment of 1^- by (a) a One-Photon Process at 266 nm and (b) a Two-Photon Process at 355 nm[a]

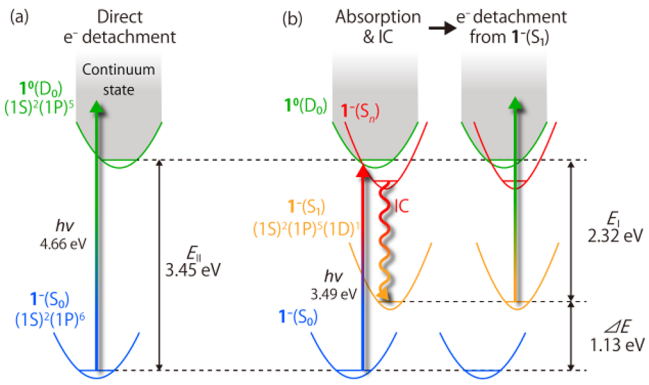

[a]For the sake of simplicity, panel b depicts only the IC process between the vibrationally ground states and the subsequent PE detachment processes.

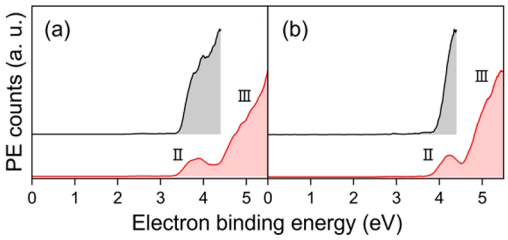

Figure 3. One-photon PE spectra of (a) 1^- and (b) 2^- measured at 266 nm (black) and 193 nm (red).

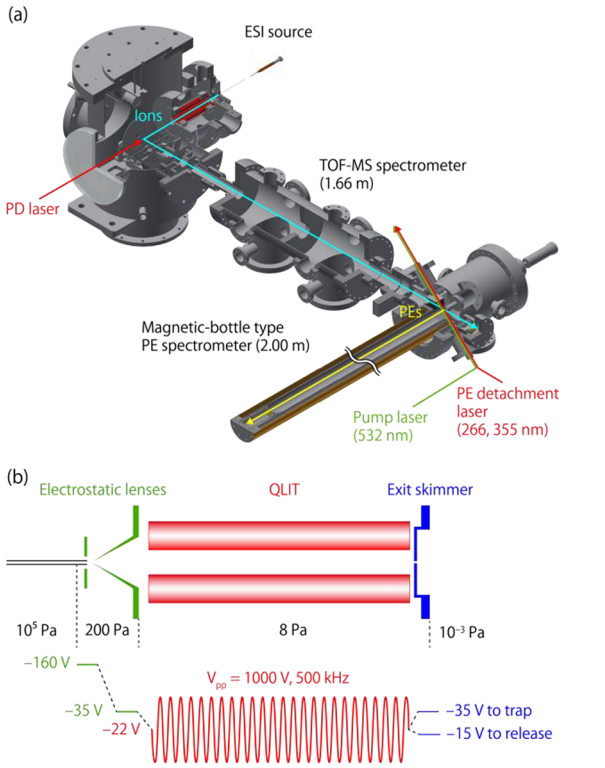

Figure 4. (a) Schematic picture of the apparatus. (b) Schematic diagram of the implemented ESI interface. Continuous ions accumulated in the QLIT and were released 300 μs before their acceleration to the TOF-MS.

had a profile different from that at 193 nm in the E_{eb} region of >3.8 eV due to the additional contribution of thermionic emission from the vibrationally excited states of 1^-, populated by rapid internal conversion (IC).[32] In conclusion, we increased the AEA of 1^0 from 2.36 ± 0.01 to 3.45 ± 0.06 eV (Table 1), which is closer to the calculated values (2.94[29] and 3.23 eV[30]) than that reported previously.[14]

The most probable scenario for a two-photon process for band I at 355 nm is the PE detachment from a photoexcited state (Scheme 1b) as observed in $[Ag_{29}(BDT)_{12}]^{3-}$ (BDT = 1,3-$S_2C_6H_4$).[17] First, cluster 1^- in the S_0 ground state is photoexcited to the S_n state, which is located at the threshold region of the PE detachment. This photoabsorption is followed by a rapid IC to 1^{-*} in the first electronically excited state (S_1). Then, the second photon in the same laser pulse detaches the electron from 1^{-*}, yielding 1^0 in the doublet state (D_0). The involvement of the S_1 state in the PE process is supported by the previous reports on the photophysical properties of 1^- in solution; the S_n states populated underwent IC within 10 ps[33,34] to S_1 whose lifetime was ~10^2 ns.[35,36] To confirm that band I originated from the electronically excited state, we conducted pump−probe PES on 1^- using two nanosecond lasers (Figure 4a and Supporting Information); 1^- was photoexcited to 1^{-*} by the pump laser (532 nm), followed by PE detachment by the probe laser (266 nm). The delay time between the pump and probe lights was controlled by the time delay of the trigger pulses to the pump and probe lasers. The intensity of band I increased when the pump and probe lights overlapped in time but decayed with the delay time of the probe light with respect to the pump light (Figure S3). This result indicates that 1^{-*} populated by the pump laser had a lifetime of >1 ns. In contrast, for naked Au[37,38] and Ag[39] cluster anions, the PE detachment via electronically excited states was rarely observed using a nanosecond laser but was observed with a femtosecond laser. The increased lifetimes of the electronically excited states of 1^- may have originated from the suppression of nonradiative relaxation by ligation-induced core rigidification, as supported by the emergence of the photoluminescence.[40,41]

The interpretation of the two-photon PE spectra, including band I and weak signals between bands I and II, is not simple because important factors such as the shape of the potential surfaces and the population of vibrational states are unknown. A hot band profile was not observed in the lower E_{eb} region of band I, although $1^-(S_1)$ is more likely to be populated in the vibrationally excited states due to lower efficiency of cooling in the gas phase than in solution. This suggests that band I is assigned to the PE detachment from the vibrationally ground state of the S_1 state. Under this assumption, the energy difference (ΔE) between E_I and E_{II} corresponds to that between the vibrationally ground states of $1^-(S_1)$ and $1^-(S_0)$ (Scheme 1b). The ΔE value of 1.13 eV (Table 2) was smaller than the optical HOMO−LUMO gap (E_{HL}) of 1.36 eV determined from the onset of the absorption spectrum (Figure S1b), indicating rapid structural relaxation in the S_1 state before the subsequent PE detachment. Within the framework of this model, the weak PE signals between bands I and II can be assigned to PE detachment from the vibrationally excited states of $1^-(S_0)$ in the electronically ground state populated by the IC from $1^-(S_1)$.

Another possible two-photon process is the PE detachment from fragment anions generated by the first photon.[42] To

https://doi.org/10.1021/acs.jpclett.2c01284
J. Phys. Chem. Lett. 2022, 13, 5049−5055

Table 2. Summary of Energetics

cluster	E_I (eV)	E_{II} (eV)	ΔE (eV)[a]	E_{HL} (eV)[b]
$[Au_{25}(PET)_{18}]^-$ ($\mathbf{1}^-$)	2.32	3.45	1.13	1.36
$[Ag_{25}(DMBT)_{18}]^-$ ($\mathbf{2}^-$)	2.66	3.97	1.31	1.54
$[AuAg_{24}(DMBT)_{18}]^-$ ($\mathbf{3}^-$)	2.52	4.00	1.48	1.60
$[PdAg_{24}(DMBT)_{18}]^{2-}$ ($\mathbf{4}^{2-}$)	0.67	2.00	1.33	1.59
$[PtAg_{24}(DMBT)_{18}]^{2-}$ ($\mathbf{5}^{2-}$)	0.56	2.08	1.52	1.68
$[PdAu_{24}(C{\equiv}CAr^F)_{18}]^{2-}$ ($\mathbf{6}^{2-}$)	2.07	3.20	1.13	1.15

[a] $\Delta E = E_{II} - E_I$. [b] Determined by the onset of the optical spectra (Figure S1b).

check such a possibility, photodissociation (PD) mass spectra of $\mathbf{1}^-$ were recorded via irradiation with a 266 nm laser 1 μs before the pulsed injection of ions into the TOF-MS (Figure 4a). The differential mass spectra with and without the PD laser (Figure S4) showed the depletion of $\mathbf{1}^-$ and the generation of a small amount (<10% of the $\mathbf{1}^-$ depletion) of $[Au_x(PET)_y]^-$ with $(x, y) = (0, 2), (1, 2), (2, 2)$, and $(2, 3)$. This result suggests that the PD was a minor process compared to PE detachment at 266 nm. In addition, the E_I value (2.32 eV) could not be explained by the AEAs of $[Au(SCH_3)_2]^0$ and $[Au_2(SCH_3)_3]^0$ (3.33 and 4.06 eV, respectively).[43]

Thus, we concluded that band I was not assigned to the PE signals from photofragments, but to those from $\mathbf{1}^{-*}$. PE spectra of other ligand-protected metal clusters may also involve the PE detachment via photoexcited states because the lifetimes are generally longer than the nanosecond order. Therefore, the dependence of the PE spectrum on the laser wavelength and fluence should be studied at least to assign a direct PE signal.

The PE spectra of the other singly charged anions, $\mathbf{2}^-$ and $\mathbf{3}^-$, measured at 266 nm at different laser fluences are shown in panels b and c of Figure 1, respectively. The spectral profiles of $\mathbf{2}^-$ and $\mathbf{3}^-$ are quite similar, indicating that the electronic structure of the Ag_{13} superatom is not appreciably affected by the replacement of a central Ag atom with a Au atom. The spectra exhibited a main band in the E_{eb} region of >4 eV (band II) with a small band in the lower-E_{eb} region (band I). The E_I and E_{II} values are summarized in Table 2. As in the case of $\mathbf{1}^-$, the relative intensity of band I to band II was smaller at a lower laser fluence. When $\mathbf{2}^-$ was irradiated at 355 nm with a fluence of 150 mJ cm^{-2}, the E_I value was further reduced to 2.07 eV (Figure S5), which agrees with the reported AEA value.[15] These results indicate that band I that appears in the low-E_{eb} region reported here and previously[15] is associated with multiphoton processes. A comparison with the PE spectrum at 193 nm (Figure 3b) confirmed that band II of $\mathbf{2}^-$ in Figure 1b was not due to the residue of background noise but is assigned to the PE signals from the HOMO (1P superatomic orbital); the AEAs of $\mathbf{2}^0$ and $\mathbf{3}^0$ were redetermined to be 3.97 and 4.00 eV, respectively, from the corresponding E_{II} values (Table 1). The newly determined AEAs of $\mathbf{2}^0$ and $\mathbf{3}^0$ are much larger than those previously reported (2.02 and 2.08 eV,[15] respectively) but are closer to the calculated values (3.46 and 3.51 eV[15], respectively). The ΔE values of $\mathbf{2}^-$ and $\mathbf{3}^-$ are slightly smaller than the corresponding E_{HL} values (Table 2), suggesting structural relaxation in the electronically excited states before PE detachment. It is noteworthy that $\mathbf{1}^0$–$\mathbf{3}^0$ can be categorized as superhalogens because their AEA values are comparable to or larger than those of halogen atoms (3.06–3.62 eV)[44] and a well-known superhalogen Al_{13} (3.57 eV).[45−47]

The PE spectra of doubly charged anions $\mathbf{4}^{2-}$–$\mathbf{6}^{2-}$ recorded at 266 nm are presented in panels d–f of Figure 1, respectively. In all cases, the PE signals were suppressed in the high-E_{eb} region because the PE detachment from deeper orbitals was hindered by the RCB created by electrostatic repulsion between the detached electron and the remaining anion.[27,28] The heights of the RCB are estimated to be ∼1.4 eV from the difference between the photon energy (4.66 eV) and the E_{eb} value at the top of band III. The PE spectra of $\mathbf{4}^{2-}$ and $\mathbf{5}^{2-}$ are similar in shape, indicating the similar electronic structures of the $Pd@Ag_{12}$ and $Pt@Ag_{12}$ superatoms. The PE spectra of $\mathbf{4}^{2-}$ and $\mathbf{5}^{2-}$ exhibit a main band with a peak at an E_{eb} of ∼3.3 eV (band III) and a hump (band II) with E_{II} values of 2.00 and 2.08 eV, respectively (Table 2). Bands II and III are assigned to PE detachment from the 1P superatomic orbital and Ag(4d) bands, respectively. On the contrary, additional bands (band I) with onset energies of 0.67 and 0.56 eV at 355 nm (Table 2) and band IV with an onset energy of ∼4 eV at 266 nm were observed in the spectra recorded at a fluence of 25 mJ cm^{-2} (Figure 1d,e), as reported previously.[15] The laser fluence dependence indicates that bands I and IV in the spectra of $\mathbf{4}^{2-}$ and $\mathbf{5}^{2-}$ are associated with two-photon processes. Band I is assigned to PE detachment from photoexcited states (Scheme 2a), as in the case of $\mathbf{1}^-$–$\mathbf{3}^-$. Band IV cannot be assigned to the

Scheme 2. Illustration of the Two-Photon Electron Detachment of $\mathbf{4}^{2-}$ via (a) $\mathbf{4}^{2-*}$ in an Electronically Excited State and (b) Singly Charged Anion $\mathbf{4}^{-}$[a]

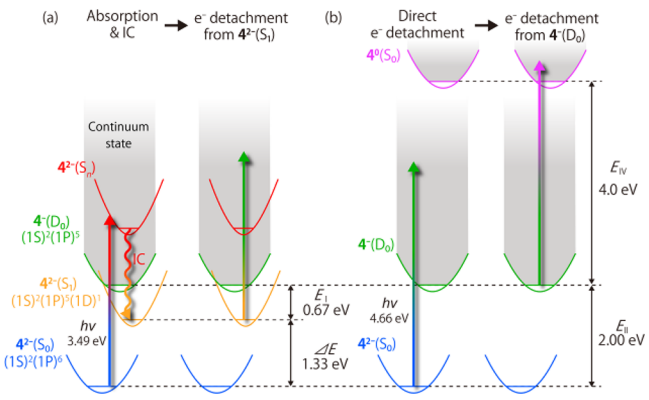

[a] For the sake of simplicity, panel a depicts only the IC process between the vibrationally ground states and the subsequent PE detachment processes.

PE detachment from doubly charged anions because the RCB with a height of ∼1.4 eV prohibits the emission of such slow electrons. The most probable assignment of band IV is PE detachment from singly charged anions such as $\mathbf{4}^-$ and $\mathbf{5}^-$ produced by the PE detachment of $\mathbf{4}^{2-}$ and $\mathbf{5}^{2-}$, respectively (Scheme 2b). In conclusion, we redetermined the AEAs of $\mathbf{4}^-$ and $\mathbf{5}^-$ to be 2.00 and 2.08 eV, respectively (Table 1), from the E_{II} values. The newly determined AEAs of $\mathbf{4}^-$ and $\mathbf{5}^-$ support the theoretical prediction that the AEA of $\mathbf{2}^0$ (3.46 eV) is reduced by ∼2.2 eV upon the doping of a single Pd or Pt atom. As discussed previously,[15] the superatomic 1P orbitals of the $M@Ag_{12}$ core are destabilized by replacing the central Ag^+ atom with the Pd^0/Pt^0 atom due to the decreased net charge of the core.

Similar discussions about the laser fluence dependence of the PE spectrum of $\mathbf{6}^{2-}$ at 266 nm (Figure 1f) led us to conclude that the E_{II} value [3.20 eV (Table 1)] corresponds to

https://doi.org/10.1021/acs.jpclett.2c01284
J. Phys. Chem. Lett. 2022, 13, 5049−5055

the AEA of $\mathbf{6}^-$. The AEA of $\mathbf{6}^-$ having a Pd@Au_{12} core was 1.12 eV larger than that of $\mathbf{5}^-$ having a Pd@Ag_{12} core. Such a large difference seems to be inconsistent with the compatibility between Au and Ag observed in $\mathbf{1}^-$−$\mathbf{3}^-$ but is explained by the electronic stabilization by the polar CF_3 groups of the ligand layer.[20] The AEAs of $\mathbf{6}^-$ after ligand exchange with C≡CPh were redetermined from the onsets of band II estimated by fitting the data in ref 20 with a Gaussian function. The newly determined AEAs are plotted against the number of C≡CPh ligands (x) in Figure S6. The AEAs decreased by 89 ± 1 meV with a single increase in x as observed in the previous paper.[20] The linear extrapolation of the plot revised the AEA of $[PdAu_{24}(C{\equiv}CPh)_{18}]^-$ from 0.73 to 1.67 eV.

In summary, we revisited the AEAs of ligand-protected icosahedral 13-atom superatoms by using an improved PES apparatus with a highly intensified ion beam. It was found that the AEAs reported previously were underestimated due to the involvement of PE detachment via photoexcited states. Although the newly determined AEAs were 1−2 eV larger than those reported previously, the qualitative effects of the doping and ligation on the AEAs of the superatoms were not affected. This study provides intrinsic information about the electronic structures and photoinduced processes of ligand-protected metal superatoms, which is useful for explaining and designing their specific properties.

■ METHODS

Samples of $\mathbf{1}^-$−$\mathbf{6}^{2-}$ were synthesized according to the previous reports (Supporting Information).[21−26] High purities of the samples were confirmed by ESI-MS and ultraviolet−visible absorption spectroscopy (Figure S1). The PES apparatus used in this study consists of an ESI source, a quadrupole linear ion trap (QLIT), a TOF-MS, and a magnetic bottle type photoelectron spectrometer with a flight path of 2.00 m (MB-PES) (Figure 4a).[20] Briefly, the cluster anions from the ESI source were desolvated by passing through a heated capillary, after which they were introduced into the QLIT (Figure 4b). After ∼98 ms in the QLIT, the ions were transferred to the acceleration region of the TOF-MS by decreasing the voltage applied to the exit aperture. After ejection for ∼300 μs, the cluster anions were accelerated perpendicularly by applying a pulsed voltage of −13 kV to the parallel electrode and then injected into the TOF-MS. After mass selection, the ions of interest without deceleration were irradiated with the third or fourth harmonic of a Nd:YAG laser (355 or 266 nm, respectively; GCR-130) operated at 10 Hz or an ArF excimer laser (193 nm, PSX-100) operated at 50 Hz. The photoelectrons emitted to all solid angles were collected and guided to the detector by an inhomogeneous magnetic field in the MB-PES. Raw TOF data were recorded by a multichannel scaler with a bin width of 5 ns. The background PE signals observed especially in the E_{eb} region of >4 eV were removed by subtracting the spectra without the ion beam from those with the ion beam. These spectra were recorded simultaneously by operating the TOF-MS at half of the laser repetition rate to minimize the effect of temporal fluctuations of the laser fluence. Finally, the TOF spectra were converted to PE spectra as a function of E_{eb} by Jacobian conversion. E_{eb} was obtained by subtracting the kinetic energy of electrons from the photon energy. The PE spectra were calibrated by using that of I^- and then smoothed by averaging the data points in the range of ±50 meV. The typical energy resolution was ∼110 meV for an electron with a kinetic energy of 1 eV. The onset of the spectrum was determined by the linear extrapolation of the spectral onset to the baseline. The integration time required to obtain one spectrum could be remarkably reduced from several hours to several minutes via the introduction of the QLIT. This improvement enabled us not only to obtain the PE spectra with a higher S/N ratio but also to study the laser fluence dependence of the PE signals for determining the number of the photons involved in the PE detachment.

■ ASSOCIATED CONTENT

Supporting Information

The Supporting Information is available free of charge at https://pubs.acs.org/doi/10.1021/acs.jpclett.2c01284.

Details about syntheses, characterization, measurements, and analysis (PDF)

Transparent Peer Review report available (PDF)

■ AUTHOR INFORMATION

Corresponding Author

Tatsuya Tsukuda − *Department of Chemistry, Graduate School of Science, The University of Tokyo, Tokyo 113-0033, Japan*; orcid.org/0000-0002-0190-6379; Email: tsukuda@chem.s.u-tokyo.ac.jp

Authors

Shun Ito − *Department of Chemistry, Graduate School of Science, The University of Tokyo, Tokyo 113-0033, Japan*

Yuriko Tasaka − *Department of Chemistry, Graduate School of Science, The University of Tokyo, Tokyo 113-0033, Japan*

Katsunosuke Nakamura − *Department of Chemistry, Graduate School of Science, The University of Tokyo, Tokyo 113-0033, Japan*

Yuki Fujiwara − *Department of Chemistry, Graduate School of Science, The University of Tokyo, Tokyo 113-0033, Japan*

Keisuke Hirata − *Laboratory for Chemistry and Life Science, Institute of Innovative Research, Tokyo Institute of Technology, Yokohama 226-8503, Japan; Department of Chemistry, School of Science, Tokyo Institute of Technology, Tokyo 152-8550, Japan; Tokyo Tech World Research Hub Initiative (WRHI), Institute of Innovation Research, Tokyo Institute of Technology, Yokohama 226-8503, Japan*

Kiichirou Koyasu − *Department of Chemistry, Graduate School of Science, The University of Tokyo, Tokyo 113-0033, Japan*; orcid.org/0000-0002-9106-0054

Complete contact information is available at: https://pubs.acs.org/10.1021/acs.jpclett.2c01284

Notes

The authors declare no competing financial interest.

■ ACKNOWLEDGMENTS

This research was financially supported by JST, CREST (Grant JPMJCR20B2), and JSPS KAKENHI (Grants JP20H00370 and JP21J20631).

■ REFERENCES

(1) Tsukuda, T.; Häkkinen, H. *Protected Metal Clusters: From Fundamentals to Applications*, 1st ed.; Elsevier B.V.: Amsterdam, 2015.

(2) Jin, R.; Zeng, C.; Zhou, M.; Chen, Y. Atomically Precise Colloidal Metal Nanoclusters and Nanoparticles: Fundamentals and Opportunities. *Chem. Rev.* **2016**, *116*, 10346−10413.

(3) Chakraborty, I.; Pradeep, T. Atomically Precise Clusters of Noble Metals: Emerging Link between Atoms and Nanoparticles. *Chem. Rev.* **2017**, *117*, 8208−8271.
(4) Yao, Q.; Yuan, X.; Chen, T.; Leong, D. T.; Xie, J. Engineering Functional Metal Materials at the Atomic Level. *Adv. Mater.* **2018**, *30*, 1802751.
(5) Du, Y.; Sheng, H.; Astruc, D.; Zhu, M. Atomically Precise Noble Metal Nanoclusters as Efficient Catalysts: A Bridge between Structure and Properties. *Chem. Rev.* **2020**, *120*, 526−622.
(6) Kang, X.; Li, Y.; Zhu, M.; Jin, R. Atomically Precise Alloy Nanoclusters: Syntheses, Structures, and Properties. *Chem. Soc. Rev.* **2020**, *49*, 6443−6514.
(7) Omoda, T.; Takano, S.; Tsukuda, T. Toward Controlling the Electronic Structures of Chemically Modified Superatoms of Gold and Silver. *Small* **2020**, *16*, 2001439.
(8) Hirai, H.; Ito, S.; Takano, S.; Koyasu, K.; Tsukuda, T. Ligand-Protected Gold/Silver Superatoms: Current Status and Emerging Trends. *Chem. Sci.* **2020**, *11*, 12233−12248.
(9) Kawawaki, T.; Ebina, A.; Hosokawa, Y.; Ozaki, S.; Suzuki, D.; Hossain, S.; Negishi, Y. Thiolate-Protected Metal Nanoclusters: Recent Development in Synthesis, Understanding of Reaction, and Application in Energy and Environmental Field. *Small* **2021**, *17*, 2005328.
(10) Takano, S.; Tsukuda, T. Chemically Modified Gold/Silver Superatoms as Artificial Elements at Nanoscale: Design Principles and Synthesis Challenges. *J. Am. Chem. Soc.* **2021**, *143*, 1683−1698.
(11) Walter, M.; Akola, J.; Lopez-Acevedo, O.; Jadzinsky, P. D.; Calero, G.; Ackerson, C. J.; Whetten, R. L.; Grönbeck, H.; Häkkinen, H. A Unified View of Ligand-Protected Gold Clusters as Superatom Complexes. *Proc. Natl. Acad. Sci. U. S. A.* **2008**, *105*, 9157−9162.
(12) Jena, P.; Sun, Q. *Superatoms: Principles, Synthesis and Applications*, 1st ed.; Wiley, 2021.
(13) Hirata, K.; Yamashita, K.; Muramatsu, S.; Takano, S.; Ohshimo, K.; Azuma, T.; Nakanishi, R.; Nagata, T.; Yamazoe, S.; Koyasu, K.; Tsukuda, T. Anion Photoelectron Spectroscopy of Free $[Au_{25}(SC_{12}H_{25})_{18}]^-$. *Nanoscale* **2017**, *9*, 13409−13412.
(14) Hirata, K.; Kim, K.; Nakamura, K.; Kitazawa, H.; Hayashi, S.; Koyasu, K.; Tsukuda, T. Photoinduced Thermionic Emission from $[M_{25}(SR)_{18}]^-$ (M = Au, Ag) Revealed by Anion Photoelectron Spectroscopy. *J. Phys. Chem. C* **2019**, *123*, 13174−13179.
(15) Kim, K.; Hirata, K.; Nakamura, K.; Kitazawa, H.; Hayashi, S.; Koyasu, K.; Tsukuda, T. Elucidating the Doping Effect on the Electronic Structure of Thiolate-Protected Silver Superatoms by Photoelectron Spectroscopy. *Angew. Chem., Int. Ed.* **2019**, *58*, 11637−11641.
(16) Hirata, K.; Tomihara, R.; Kim, K.; Koyasu, K.; Tsukuda, T. Characterization of Chemically Modified Gold and Silver Clusters in Gas Phase. *Phys. Chem. Chem. Phys.* **2019**, *21*, 17463−17474.
(17) Veenstra, A. P.; Monzel, L.; Baksi, A.; Czekner, J.; Lebedkin, S.; Schneider, E. K.; Pradeep, T.; Unterreiner, A.-N.; Kappes, M. M. Ultrafast Intersystem Crossing in Isolated $Ag_{29}(BDT)_{12}^{3-}$ Probed by Time-Resolved Pump−Probe Photoelectron Spectroscopy. *J. Phys. Chem. Lett.* **2020**, *11*, 2675−2681.
(18) Tasaka, Y.; Nakamura, K.; Malola, S.; Hirata, K.; Kim, K.; Koyasu, K.; Häkkinen, H.; Tsukuda, T. Electron Binding in a Superatom with a Repulsive Coulomb Barrier: The Case of $[Ag_{44}(SC_6H_3F_2)_{30}]^{4-}$ in the Gas Phase. *J. Phys. Chem. Lett.* **2020**, *11*, 3069−3074.
(19) Koyasu, K.; Tsukuda, T. Gas-Phase Studies of Chemically Synthesized Au and Ag Clusters. *J. Chem. Phys.* **2021**, *154*, 140901.
(20) Ito, S.; Koyasu, K.; Takano, S.; Tsukuda, T. Critical Role of CF_3 Groups in the Electronic Stabilization of $[PdAu_{24}(C{\equiv}CC_6H_3(CF_3)_2)_{18}]^{2-}$ as Revealed by Gas-Phase Anion Photoelectron Spectroscopy. *J. Phys. Chem. Lett.* **2021**, *12*, 10417−10421.
(21) Heaven, M. W.; Dass, A.; White, P. S.; Holt, K. M.; Murray, R. W. Crystal Structure of the Gold Nanoparticle $[N(C_8H_{17})_4]$-$[Au_{25}(SCH_2CH_2Ph)_{18}]$. *J. Am. Chem. Soc.* **2008**, *130*, 3754−3755.
(22) Zhu, M.; Aikens, C. M.; Hollander, F. J.; Schatz, G. C.; Jin, R. Correlating the Crystal Structure of A Thiol-Protected Au_{25} Cluster and Optical Properties. *J. Am. Chem. Soc.* **2008**, *130*, 5883−5885.
(23) Joshi, C. P.; Bootharaju, M. S.; Alhilaly, M. J.; Bakr, O. M. $[Ag_{25}(SR)_{18}]^-$: The "Golden" Silver Nanoparticle. *J. Am. Chem. Soc.* **2015**, *137*, 11578−11581.
(24) Yan, J.; Su, H.; Yang, H.; Malola, S.; Lin, S.; Häkkinen, H.; Zheng, N. Total Structure and Electronic Structure Analysis of Doped Thiolated Silver $[MAg_{24}(SR)_{18}]^{2-}$ (M = Pd, Pt) Clusters. *J. Am. Chem. Soc.* **2015**, *137*, 11880−11883.
(25) Bootharaju, M. S.; Joshi, C. P.; Parida, M. R.; Mohammed, O. F.; Bakr, O. M. Templated Atom-Precise Galvanic Synthesis and Structure Elucidation of a $[Ag_{24}Au(SR)_{18}]^-$ Nanocluster. *Angew. Chem., Int. Ed.* **2016**, *55*, 922−926.
(26) Takano, S.; Ito, S.; Tsukuda, T. Efficient and Selective Conversion of Phosphine-Protected $(MAu_8)^{2+}$ (M = Pd, Pt) Superatoms to Thiolate-Protected $(MAu_{12})^{6+}$ or Alkynyl-Protected $(MAu_{12})^{4+}$ Superatoms via Hydride Doping. *J. Am. Chem. Soc.* **2019**, *141*, 15994−16002.
(27) Wang, L.-S.; Wang, X.-B. Probing Free Multiply Charged Anions Using Photodetachment Photoelectron Spectroscopy. *J. Phys. Chem. A* **2000**, *104*, 1978−1990.
(28) Dau, P. D.; Liu, H.-T.; Yang, J.-P.; Winghart, M.-O.; Wolf, T. J. A.; Unterreiner, A.-N.; Weis, P.; Miao, Y.-R.; Ning, C.-G.; Kappes, M. M.; Wang, L.-S. Resonant Tunneling through the Repulsive Coulomb Barrier of a Quadruply Charged Molecular Anion. *Phys. Rev. A* **2012**, *85*, 064503.
(29) Jung, J.; Kang, S.; Han, Y.-K. Ligand Effects on the Stability of Thiol-Stabilized Gold Nanoclusters: $Au_{25}(SR)_{18}^-$, $Au_{38}(SR)_{24}$, and $Au_{102}(SR)_{44}$. *Nanoscale* **2012**, *4*, 4206−4210.
(30) Matus, M. F.; Malola, S.; Kinder Bonilla, E.; Barngrover, B. M.; Aikens, C. M.; Häkkinen, H. A Topological Isomer of the $Au_{25}(SR)_{18}^-$ Nanocluster. *Chem. Commun.* **2020**, *56*, 8087−8090.
(31) Wang, L.-S.; Ding, C.-F.; Wang, X.-B.; Barlow, S. E. Photodetachment Photoelectron Spectroscopy of Multiply Charged Anions Using Electrospray Ionization. *Rev. Sci. Instrum.* **1999**, *70*, 1957−1966.
(32) Hirata, K.; Ito, S.; Kim, K.; Nakamura, K.; Kitazawa, H.; Hayashi, S.; Koyasu, K.; Tsukuda, T. Correction to Photoinduced Thermionic Emission from $[M_{25}(SR)_{18}]^-$ (M = Au, Ag) Revealed by Anion Photoelectron Spectroscopy. *J. Phys. Chem. C* **2022**, *126*, 8965−8966.
(33) Miller, S. A.; Womick, J. M.; Parker, J. F.; Murray, R. W.; Moran, A. M. Femtosecond Relaxation Dynamics of $Au_{25}L_{18}^-$ Monolayer-Protected Clusters. *J. Phys. Chem. C* **2009**, *113*, 9440−9444.
(34) Green, T. D.; Knappenberger, K. L. Relaxation Dynamics of $Au_{25}L_{18}$ Nanoclusters Studied by Femtosecond Time-Resolved Near Infrared Transient Absorption Spectroscopy. *Nanoscale* **2012**, *4*, 4111−4118.
(35) Wu, Z.; Jin, R. On the Ligand's Role in the Fluorescence of Gold Nanoclusters. *Nano Lett.* **2010**, *10*, 2568−2573.
(36) Zhou, M.; Song, Y. Origins of Visible and Near-Infrared Emissions in $[Au_{25}(SR)_{18}]^-$ Nanoclusters. *J. Phys. Chem. Lett.* **2021**, *12*, 1514−1519.
(37) Niemietz, M.; Gerhardt, P.; Ganteför, G.; Dok Kim, Y. Relaxation Dynamics of the Au_3^- and Au_6^- Cluster Anions. *Chem. Phys. Lett.* **2003**, *380*, 99−104.
(38) Walter, M.; Häkkinen, H.; Stanzel, J.; Neeb, M.; Eberhardt, W. Symmetry-Induced Long-Lived Excited State in Au_6^-. *Phys. Rev. B* **2007**, *76*, 155422.
(39) Niemietz, M.; Engelke, M.; Kim, Y. D.; Ganteför, G. Electronic Relaxation in Ag Nanoclusters Studied with Time-Resolved Photoelectron Spectroscopy. *Phys. Rev. B* **2007**, *75*, 085438.
(40) Pyo, K.; Thanthirige, V. D.; Kwak, K.; Pandurangan, P.; Ramakrishna, G.; Lee, D. Ultrabright Luminescence from Gold Nanoclusters: Rigidifying the Au(I)−Thiolate Shell. *J. Am. Chem. Soc.* **2015**, *137*, 8244−8250.

https://doi.org/10.1021/acs.jpclett.2c01284
J. Phys. Chem. Lett. 2022, 13, 5049−5055

(41) Kang, X.; Zhu, M. Tailoring the Photoluminescence of Atomically Precise Nanoclusters. *Chem. Soc. Rev.* **2019**, *48*, 2422−2457.
(42) Ganteför, G.; Kraus, S.; Eberhardt, W. Femtosecond Photoelectron Spectroscopy of the Photodissociation of Au_3^-. *J. Electron Spectrosc. Relat. Phenom.* **1998**, *88−91*, 35−40.
(43) Ning, C.-G.; Xiong, X.-G.; Wang, Y.-L.; Li, J.; Wang, L.-S. Probing the Electronic Structure and Chemical Bonding of the "Staple" Motifs of Thiolate Gold Nanoparticles: $Au(SCH_3)_2^-$ and $Au_2(SCH_3)_3^-$. *Phys. Chem. Chem. Phys.* **2012**, *14*, 9323−9329.
(44) Gutsev, G. L.; Boldyrev, A. I. DVM-Xα Calculations on the Ionization Potentials of MX_{k+1}^- Complex Anions and the Electron Affinities of MX_{k+1} "Superhalogens". *Chem. Phys.* **1981**, *56*, 277−283.
(45) Li, X.; Wang, L.-S. Experimental Search and Characterization of Icosahedral Clusters: $Al_{12}X^-$ (X = C, Ge, Sn, Pb). *Phys. Rev. B* **2002**, *65*, 153404.
(46) Bergeron, D. E.; Castleman, A. W., Jr.; Morisato, T.; Khanna, S. N. Formation of $Al_{13}I^-$: Evidence for the Superhalogen Character of Al13. *Science* **2004**, *304*, 84−87.
(47) Reber, A. C.; Khanna, S. N.; Castleman, A. W. Superatom Compounds, Clusters, and Assemblies: Ultra Alkali Motifs and Architectures. *J. Am. Chem. Soc.* **2007**, *129*, 10189−10194.

https://doi.org/10.1021/acs.jpclett.2c01284
J. Phys. Chem. Lett. 2022, 13, 5049−5055